energies

Article

An Improvement of Holistic Control Tuning for Reducing Energy Consumption in Seamless Transitions for a BESS Grid-Connected Converter

Alberto Arellanes [1], Ciro Nuñez [1,*], Nancy Visairo [1] and Andres A. Valdez-Fernandez [2]

[1] Facultad de Ingeniería, Universidad Autónoma de San Luis Potosí, San Luis Potosi 78290, Mexico
[2] Facultad de Ciencias, Universidad Autónoma de San Luis Potosí, San Luis Potosi 78295, Mexico
* Correspondence: calberto@uaslp.mx; Tel.: +52-444-826-2300 (ext. 6264)

Abstract: This paper presents an improvement of the tuning process of the holistic control published by the authors in previous research to achieve a seamless transition among three operation mode changes and load transients. The proposed tuning approach reveals an improvement in the energy consumption of the Battery Energy Storage System (BESS) during all operation mode transients compared to the holistic control. For this aim, the system addressed is a BESS with the capability to ride through three operation modes of interest: the grid-connected mode as an inverter, the grid-connected mode as a rectifier, and the islanded operation mode. The LCL filter design by using the Butterworth polynomial approach is presented in more detail, and its smooth inherent transient response is preserved when the tuning of the controller gains is carried out by using the same polynomial approach but now including the integral action within the Butterworth polynomial. To reveal the reduction in energy consumption, the closed-loop transfer functions of each mode were used to compare the previous holistic control and this new one named by the authors as the "improved holistic control". The closed-loop system fulfills the frequency and voltage thresholds of the IEEE 1547-2018 standard seamlessly. The simulation runs were conducted on the PSCAD/EMTDC to evaluate the seamless transition among the operation mode changes and load steps. The experimental results in a 617 W, 120 V_{L-L} three-phase converter prototype are included to demonstrate the validity of the improved holistic control.

Keywords: seamless transition; BESS; grid-connected mode; islanded mode; LCL-filter; holistic control

check for updates

Citation: Arellanes, A.; Nuñez, C.; Visairo, N.; Valdez-Fernandez, A.A. An Improvement of Holistic Control Tuning for Reducing Energy Consumption in Seamless Transitions for a BESS Grid-Connected Converter. *Energies* **2022**, *15*, 7964. https://doi.org/10.3390/en15217964

Academic Editors: Bharatiraja Chokkalingam and Lucian Mihet-Popa

Received: 20 September 2022
Accepted: 21 October 2022
Published: 27 October 2022

1. Introduction

With the addition of renewable energy as the distributed generation in the power system and its intermittent nature, the energy storage is becoming a vital factor for the capacity firming for renewable energy sources. Currently, pumped hydroelectric storage is still the most widely used. However, the BESS has increasingly received attention due mainly to its low cost and improved performance [1,2]. The BESS can provide different services, such as bulk energy, ancillary services, grid system improvement, customer energy management, transport sector, and islanded mode [3–5]. To increase its economic feasibility, the BESS is used not only to provide one service but a combination of several services [6].

Several topics have been studied to provide a good performance when the BESS commutes among the modes related to the services that supply it. One of these topics is the control scheme. For example, in [7], the authors proposed a hierarchical control to provide the BESS with a seamless transition when multiple tasks are required for it. The hierarchical control allows the optimization of one or multiple objectives [7]. Furthermore, in [4,8,9], the authors claim that hierarchical control leads to lower operating costs while increasing the efficiency and reliability given a cost function according to the user priorities. For example, Ref. [10] proposes a Self-Adaptive Elephant Herd Optimization with a cost saving of up to 90.91%. Figure 1a shows the hierarchical control triangle used for the BESS. It can be seen that level 3 is related to the market variables, such as the cost of MXN/kWh. From this level, the output is a reference of the market power dispatch P_m^* and Q_m^*, and it applies, if it is desirable, the participation of the BESS in the electrical market. As a consequence, the references variations are the slowest. Level 2 is related to the wide-area voltage and the frequency regulation references P_r^* and Q_r^*, which contribute to the power system stability. The dynamic is faster than in the previous level due to the droop references P_{droop}^* and Q_{droop}^* that are obtained locally as in [11]. At the base of the triangle, the fastest level 0 is located, where the addition of the references activates either a voltage mode or a current mode, each one with its respective control scheme and tuning.

(a) Typical hierarchical control triangle

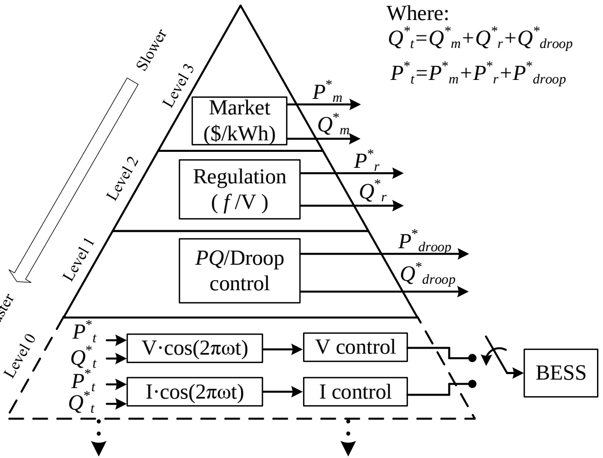

(b) Proposed holistic control

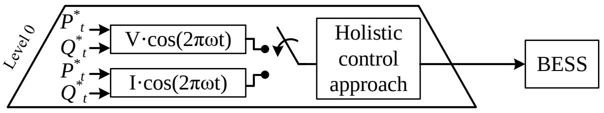

Figure 1. Control scheme: (**a**) hierarchical control [6,7] and (**b**) holistic control.

Usually, one controller is designed and tuned to maintain the output current in the phase with the AC mains voltage, and the other controller permits a sinusoidal output voltage when the islanded operation mode is required. This kind of control structure in level 0 is known as hybrid control [12–15]. Meanwhile, when the grid-connected mode is required to charge the BESS, another controller is used to make the converter work as a rectifier, which is usually not included in references devoted to the BESS [15,16].

Nevertheless, in recent years, the unification of the DC/AC power converter control has been of considerable interest, providing the ability of working in the grid-connected mode and islanded operation mode with a single control [5,17].

The unified control, which is an enhancement of the hybrid control, operates in level 0 and level 1. A modified PQ/droop control is typically used in level 1, while in level 0, a single V/I control is used, depending on whether the voltage or current is desired at the BESS output [16–18].

Likewise, a seamless transition among modes has become a critical issue to preserve the grid stability [8,19,20]. For example, in [21], an uninterruptible AC power supply is required in the case of sensitive industrial local loads, which also reduces voltage and current spikes during transients. Meanwhile, when re-connection to the grid occurs, the voltage and frequency should be maintained under standard thresholds to preserve the continuous power system operation [22]. Several efforts have addressed the unified control design with different approaches. One approach is through the Phase-Locked Loop (PLL) design or modification. Reference [20] presents a control strategy that operates the inverter in the islanded operation mode and grid-connected mode as a voltage source and a current source, respectively. The main merit of this work is to extend the PLL, which makes a smooth transition in the phase angle when it is changing between the grid reference and an independent reference. The authors in [23] present a new control scheme based on integrating the PLL in the DC/AC power converter control, in which the inverter, as an islanded operation mode, makes a pre-synchronization with the grid. This PLL does not allow hops in the angle. Another approach is through the DC/AC converter control design or modification. In [18], a control design is presented wherein a feed-forward current control is used for the grid-connected mode, whereas in the islanded operation mode, a voltage droop control strategy is used to deliver the required power to local loads. The authors of [24] use a typical control scheme of two cascade controllers into a dq-frame when the inverter is working in the grid-connected mode; in this case, the outer loop is removed when the inverter is working in the islanded operation mode. In [25], the authors propose a unified control based on a droop control strategy, which adds power compensation to realize a seamless transition among the operation modes. The key resides in the saturation of part of the controller in the islanded operation mode. It introduces a power compensation in order to behave as a typical droop control strategy. More recent evidence [26] proposes two different sets of controllers, one for the grid-connected mode as grid feeding and the other one for the islanded operation mode as grid forming. The main contribution in this work resides in the islanded operation mode where "A modified linear voltage control strategy with an output current feed-forward and capacitor current feedback gained by high pass filter". A recent review of the literature on this topic found that, usually, the design of the LCL filter and the control design are treated separately.

In [27], the control design is carried out from a holistic viewpoint to achieve a seamless transition among the different operation modes, including the battery charger mode. A seamless transition is provided by selecting a Butterworth behavior from the LCL filter design in order to guarantee smooth overshoots during transient responses. Following the same idea, the feedback-controller gain tuning is designed to preserve such specific behavior but improve the fastness of the transient response by increasing the wideband. The control design takes advantage of the main characteristics of a low-order Butterworth filter which are: a fast response and slight overshoots [28], maximally flat in the passband in the amplitude response, no passband ripple [29], and a good trade-off between the attenuation and phase response [30]. This unified control has the merit of having analyzed the performance of the three considered operation modes with a single set of controller gains. Another important characteristic of this controller is that only one feedback loop is used, unlike the typical multi-loop controllers [24]. The control scheme reported in [27] uses state feedback with an integrator where the state feedback is tuned by using the Butterworth polynomial, but the integrator is tuned separately.

In this paper, unlike the previous work, the authors propose an enhanced tuning considering the gains of the state feedback and the integrator concatenated in the same Butterworth polynomial with the objective of improving the energy consumption to ride-through from one operation mode to another. Although both tuning methods show subtle differences in the tuning process, the effect on the energy performance is remarkable, as will be revealed in this paper.

This paper is organized as follows: Section 2 describes the BESS topology and presents the three mathematical models of the three operation modes. Section 3 provides the LCL filter design guidelines to achieve seamless mode transitions in detail. Section 4 presents the improved holistic control design of the BESS system. In Section 5, a comparison of the two tuning control approaches was made regarding the energy consumed during an event. In Section 6, the simulation and experimental results are given and discussed, and the conclusions are given in Section 7.

2. Modeling of the DC/AC Converter and LCL Filter

Figure 2 shows the BESS topology with the holistic control. The BESS system is composed of the power stage in red line, sensors and control stage in green line, and the grid in black line.

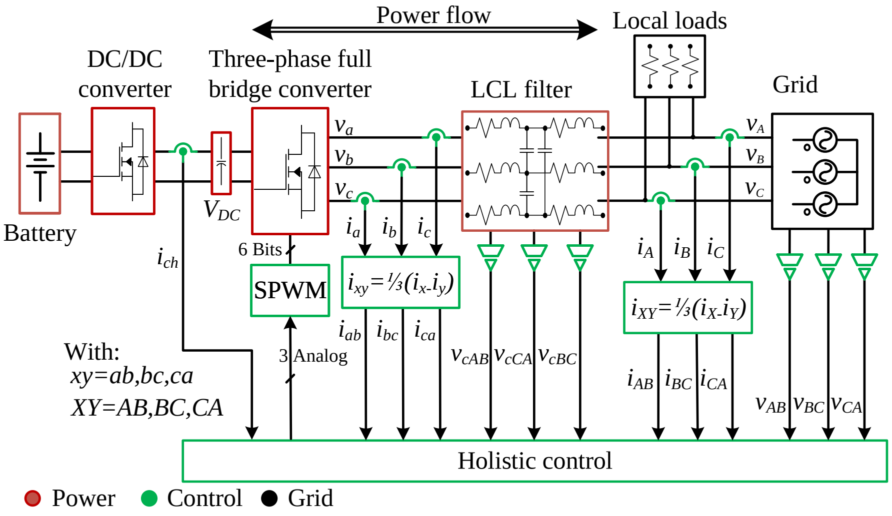

Figure 2. BESS system along with holistic control.

where:

- v_{ab}, v_{bc}, v_{ca} are the delta-connected output voltages of the power converter.
- v_{cAB}, v_{cBC}, v_{cCA} are the delta-connected capacitor voltages.
- i_a, i_b, i_c are the currents through inductors L_{f1}.
- $i_{a'b'}$, $i_{b'c'}$, $i_{c'a'}$ are the delta-connected capacitor currents.
- i_A, i_B, i_C are the currents through inductors L_{f2}.
- v_{AB}, v_{BC}, v_{CA} are the delta-connected grid voltages.

In addition, consider:

$$i_{ab} = \frac{1}{3}(i_a - i_b) \tag{1}$$

$$i_{AB} = \frac{1}{3}(i_A - i_B) \tag{2}$$

$$v_{cAB} = \frac{1}{3}(v_{a'} - v_{b'}) \tag{3}$$

The battery bank and the DC/DC converter [31] are well-modeled as an ideal DC voltage source for the three operation modes.

To obtain the mathematical models of the three operation modes, the following assumptions are considered:

1. The three-phase system is balanced.
2. A line-to-line modeling is considered.
3. The complete analysis is based on the average mathematical model.
4. The link capacitor voltage is not considered as a state variable. Additionally, the voltage V_{DC} is always bigger than the peak of line-to-line voltage.
5. The grid-connected converter works as an inverter if the currents i_{AB}, i_{BC}, and i_{CA} are in phase with the input voltages v_{AB}, v_{BC}, and v_{CA}, respectively. In this case, the active power flows from V_{DC} to the grid and the capacitor is not discharged because of the action of the DC/DC converter and the battery bank.
6. The grid-connected converter works as a rectifier if the input currents i_{AB}, i_{BC}, and i_{CA} are shifted 180° with respect to the input voltage v_{AB}, v_{BC}, and v_{CA}, respectively. In this case, the active power flows from the grid to the V_{DC}, and the capacitor is not overcharged because the DC/DC converter is charging the battery bank.

7. The analysis is performed considering the phase AB. Taking advantage of assumption (1), the rest of the control signals are obtained by shifting their phases by 120° and 240°, respectively.

The linear models considered are [27]:
(1) Islanded operation mode:

$$\begin{gathered}\begin{bmatrix} \dot{x}_1 \\ \dot{x}_2 \\ \dot{x}_3 \end{bmatrix} = \begin{bmatrix} 0 & 0 & \frac{-1}{3L_{f1}} \\ 0 & \frac{-Z_{AB}}{3L_{f2}} & \frac{1}{3L_{f2}} \\ \frac{3}{C_f} & \frac{-3}{C_f} & 0 \end{bmatrix} \begin{bmatrix} x_1 \\ x_2 \\ x_3 \end{bmatrix} + \begin{bmatrix} \frac{1}{3L_{f1}} \\ 0 \\ 0 \end{bmatrix} v_{ab} \\ \mathbf{y} = \begin{bmatrix} 0 & 0 & 1 \end{bmatrix} \begin{bmatrix} x_1 \\ x_2 \\ x_3 \end{bmatrix}\end{gathered} \tag{4}$$

(2) Grid-connected mode (inverter):

$$\begin{gathered}\begin{bmatrix} \dot{x}_1 \\ \dot{x}_2 \\ \dot{x}_3 \end{bmatrix} = \begin{bmatrix} 0 & 0 & \frac{-1}{3L_{f1}} \\ 0 & \frac{-Z_{AB}}{3L_{f2}} & \frac{1}{3L_{f2}} \\ \frac{3}{C_f} & \frac{-3}{C_f} & 0 \end{bmatrix} \begin{bmatrix} x_1 \\ x_2 \\ x_3 \end{bmatrix} + \begin{bmatrix} \frac{1}{3L_{f1}} \\ 0 \\ 0 \end{bmatrix} v_{ab} \\ \mathbf{y} = \begin{bmatrix} 0 & 1 & 0 \end{bmatrix} \begin{bmatrix} x_1 \\ x_2 \\ x_3 \end{bmatrix}\end{gathered} \tag{5}$$

(3) Grid-connected mode (rectifier):

$$\begin{gathered}\begin{bmatrix} \dot{x}_1 \\ \dot{x}_2 \\ \dot{x}_3 \end{bmatrix} = \begin{bmatrix} 0 & 0 & \frac{-1}{3L_{f1}} \\ 0 & 0 & \frac{1}{3L_{f2}} \\ \frac{3}{C_f} & \frac{-3}{C_f} & 0 \end{bmatrix} \begin{bmatrix} x_1 \\ x_2 \\ x_3 \end{bmatrix} + \begin{bmatrix} \frac{1}{3L_{f1}} \\ 0 \\ 0 \end{bmatrix} v_{ab} + \begin{bmatrix} 0 \\ \frac{-1}{3L_{f2}} \\ 0 \end{bmatrix} v_{AB} \\ \mathbf{y} = \begin{bmatrix} 0 & 1 & 0 \end{bmatrix} \begin{bmatrix} x_1 \\ x_2 \\ x_3 \end{bmatrix}\end{gathered} \tag{6}$$

where $\mathbf{x} = \begin{bmatrix} i_{ab} & i_{AB} & v_{cAB} \end{bmatrix}^{\mathrm{T}}$ is the state vector of dimension $n = 3$, v_{ab} is the control input of dimension $m = 1$, and $\mathbf{y}$ is the controlled output vector of dimension $p = 1$.

3. Butterworth LCL Filter Design

For showing the concatenation of the tuning control with the LCL filter design, in this paper, the design process of the filter is shown in more detail than [27]. This is responsible for maintaining the electrical requirements according to the standard IEEE-1547-2018 [22]. It is also important to highlight that this filter determines the dynamic under transients or mode transitions. In this paper, we designed the LCL filter according to the Butterworth polynomial firstly presented in [32].

For the LCL filter design using the Butterworth polynomial, the starting assumption is to consider the islanded operation mode at rated active power. This assumption is used due to the method [33] considers the rated load as a resistive load. However, the previous assumption works when the filter operates in any other operation mode because the active power capability has already been considered.

In this paper, the Butterworth filter synthesis technique described by [33] is employed to take advantage of its straightforwardness, standardized design, and practicality to be utilized for communications or grid-connected filters. First, the input parameters for designing the LCL filter using SPWM, as the modulation technique, are established:

1. Switching frequency f_{sw} = 12,060 Hz; $\omega_{sw} = 75.7$ krad/s.
2. Amplitude and frequency modulation indexes $m_a = 0.85$ and $m_f = 201$, respectively.
3. First relevant harmonic amplitude $\mathrm{h}_{199(11940\mathrm{Hz})} = 0.289$.
4. For the three-phase full-bridge converter, the double-edge naturally sampled PWM is taken for this work, and given this, the first carrier harmonic group has the more significant harmonic at $m_f - 2 = 199$ being $\omega_{h_{199}} = 75.02$ krad/s [34].
5. According to IEEE-1159, THD voltage at the connection point should be lower than 3%; to extensively fulfill this requirement, an attenuation for the first relevant harmonic was proposed of $G(jw)_{h199} = -32$ dB.
6. Rated load value $Z_{load} = Z_{AB} = 70\ \Omega$ for rated power. It is important to notice that the approach considers a resistive load; it means active power transference. Of course, the BESS operates under different modes and operating conditions, and the filter should be able to allow the transfer of the required power in both directions.

The transfer function of the Butterworth filter is given by [33]:

$$G(s) = \frac{1}{Q(s)} \tag{7}$$

where $Q(s)$ is the normalized Butterworth polynomial. Table 1 presents the first four normalized polynomials.

Table 1. Normalized Butterworth polynomials [33].

Filter Order	Polynomial $Q(s)$
1.	$s+1$
2.	$s^2 + 1.4142s + 1$
3.	$s^3 + 2.000s^2 + 2.0000s + 1$
4.	$s^4 + 2.6131s^3 + 3.4142s^2 + 2.6131s + 1$

For the LCL filter design, two additional parameters are needed: $Q(s)$ and the cut-off frequency ω_n. In this work, the third-order polynomial has been selected because there are three energy storage elements. Because the transfer function of the third-order Butterworth filter dependent on ω_n, it can be divided into a simple pole and two complex conjugate poles:

$$G(s) = \frac{\omega_n}{s+\omega_n} \frac{\omega_n^2}{s^2 + \omega_n s + \omega_n^2} \tag{8}$$

Then, the frequency response equation for magnitude, with $s = j\omega$, is given as:

$$\left|G(j\omega)_{h199}\right| = 20\log\left(\frac{\omega_n}{\sqrt{\omega_n^2 + \omega_{h_{199}}^2}} \frac{\omega_n^2}{\sqrt{\left(\omega_n^2 - \omega_{h_{199}}^2\right)^2 + (\omega_n \omega_{h_{199}})^2}}\right) \tag{9}$$

Solving ω_n from Equation (9) and given the $G(j\omega)_{h_{199}} = -32$ dB of attenuation for the first relevant harmonic $\mathrm{h}_{199(11940)}$, then ω_n is calculated as follows:

$$\omega_n = -\frac{(-1)^{5/6} \omega_{h_{199}} 10^{G(jw)_{h199}/60}}{\sqrt[6]{10^{G(jw)_{h199}/10} - 1}} \tag{10}$$

with the frequency of $\omega_n = 21.97$ krad/s, according to [33], the reference passive elements L_r and C_r can be calculated as follows:

$$L_r = \frac{Z_{load}}{\omega_n} = 3.18\,\text{mH} \tag{11}$$

$$C_r = \frac{1}{Z_{load}\omega_n} = 0.65\,\mu\text{F} \tag{12}$$

with $Z_{load} = 70\,\Omega$.

Once L_r and C_r are calculated, the LCL filter elements are:

$$L_{f1} = \frac{1.5}{3L_r} = 1.59\,\text{mH} \tag{13}$$

$$L_{f2} = \frac{0.5}{3L_r} = 530.95\,\mu\text{H} \tag{14}$$

$$C_f = 3 \times 1.3333 C_r = 2.60\,\mu\text{F} \tag{15}$$

The denormalized transfer function of the Butterworth filter is given by:

$$G(s) = \frac{v_{AB}(s)}{v_{ab}(s)} = \frac{Z_{load}}{L_{f1}C_f L_{f2}s^3 + L_{f1}C_f Z_{load}s^2 + \left(L_{f1} + L_{f2}\right)s + Z_{load}} \tag{16}$$

Figure 3 shows the Bode diagram of the third-order filter, considering the desired attenuation. Figure 3 also shows the proposed wideband which contains the candidate eigenvalues for the closed-loop system.

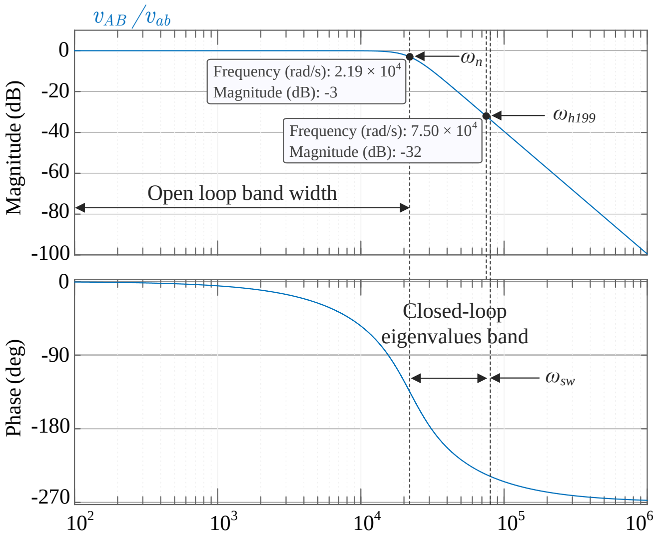

Figure 3. $G(s)$ Bode diagram in islanded mode.

Once the filter has been designed for islanded operation mode, it works for the other two operation modes, which are grid-connected mode as inverter and grid-connected mode as rectifier. This can be seen clearly in the next section.

4. Improvement of the Holistic Control Tuning

This section describes the tuning procedure to provide a complete Butterworth closed-loop system. To begin with the procedure, it is necessary to determine the open-loop eigenvalues of the three operation modes, which are summarized in Table 2.

Table 2. Open-loop matrices and eigenvalues.

Operation Mode	State Matrix	Input Matrix	Output Matrix	Eigenvalues (rad/s)
Islanded mode (ism)	$\mathbf{A}_{\text{ism}}$	$\mathbf{B}_{\text{ism}}$	$\mathbf{C}_{\text{ism}}$	$\alpha_{1\_\text{ism}} = -21.97 \times 10^3$ $\alpha_{2,3\_\text{ism}} = (-10.98 \pm \text{j}19.03) \times 10^3$
Grid-connected mode inverter (gci)	$\mathbf{A}_{\text{gci}}$	$\mathbf{B}_{\text{gci}}$	$\mathbf{C}_{\text{gci}}$	$\alpha_{1\_\text{gci}} = -21.97 \times 10^3$ $\alpha_{2,3\_\text{gci}} = (-10.98 \pm j19.03) \times 10^3$
Grid-connected mode rectifier (gcr)	$\mathbf{A}_{\text{gcr}}$	$\mathbf{B}_{\text{gcr\_1}}$ $\mathbf{B}_{\text{gcr\_2}}$	$\mathbf{C}_{\text{gcr}}$	$\alpha_{1\_\text{gcr}} = 0$ $\alpha_{2,3\_\text{gcr}} = (\pm j31.10) \times 10^3$

Table 2 highlights that the eigenvalues in islanded mode and grid-connected mode (inverter) are the same. Furthermore, it is important to note that $|\alpha_{1\_\text{ism}}|$ and $|\alpha_{1\_\text{gci}}|$ correspond to bandwidth in the same way as $|\alpha_{2,3\_\text{ism}}|$ and $|\alpha_{2,3\_\text{gci}}|$ do, implying that the grid-connected mode inverter is also Butterworth. In counterpart, it can be seen that the grid-connected mode rectifier has different eigenvalues.

Figure 4 shows the control proposal. The block diagram is the same as those reported by authors in [27]. To enhance the energy consumption of the system when mode changes and load transients occur, the authors thought to improve the closed-loop tuning by doing a complete Butterworth polynomial considering the closed-loop system (17), unlike in [27].

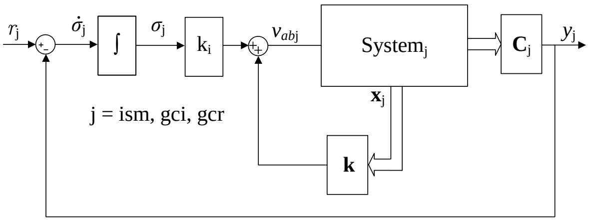

Figure 4. Block diagram of the controller.

The closed-loop system for islanded operation mode is:

$$\begin{bmatrix} \dot{\mathbf{x}} \\ \dot{\sigma}_{\text{ism}} \end{bmatrix} = \begin{bmatrix} \mathbf{A}_{\text{ism}} + \mathbf{B}_{\text{ism}}\mathbf{k} & \mathbf{B}_{\text{ism}}\text{k}_\text{i} \\ -\mathbf{C}_{\text{ism}} & 0 \end{bmatrix} \begin{bmatrix} \mathbf{x} \\ \sigma_{\text{ism}} \end{bmatrix} + \begin{bmatrix} \mathbf{0} \\ 1 \end{bmatrix} r \tag{17}$$

or

$$\begin{bmatrix} \dot{\mathbf{x}} \\ \dot{\sigma}_{\text{ism}} \end{bmatrix} = \hat{\mathbf{A}} \begin{bmatrix} \mathbf{x} \\ \dot{\sigma}_{\text{ism}} \end{bmatrix} + \begin{bmatrix} \mathbf{0} \\ 1 \end{bmatrix} r \tag{18}$$

where:

- $\mathbf{x}$ is the state vector.
- r is the reference of the controlled output.
- $\mathbf{A}_{\text{ism}}$, $\mathbf{B}_{\text{ism}}$, and $\mathbf{C}_{\text{ism}}$ are the state, input, and output matrices, respectively.
- $\dot{\sigma}_{\text{ism}}$ is the error between the voltage reference and measured voltage.
- $v_{ab_{\text{ism}}}$ is the control law which modifies the inverter output.
- $\mathbf{k}$ is the gain vector.
- k_i is the gain of the integral action.

As already proved in [27], the system is controllable, and the limits to place the closed-loop poles are $[\omega_n = 21.97\,\text{krad/s}, \omega_{sw} = 75.7\,\text{krad/s}]$ given by the open-loop LCL filter bandwidth and the switching frequency, respectively.

The eigenvalues position will be chosen in order to maintain the fourth-order Butterworth filter dynamic, unlike [27]. Based on the normalized Butterworth polynomials shown in Table 1, the poles of the transfer function will be distributed in a normalized way in the left half of a unit circle centered at the origin of the complex plane as is shown in Figure 5, according to [35]. It is important to note that the order of the system will increase by one, because an integrator is incorporated into the closed control loop.

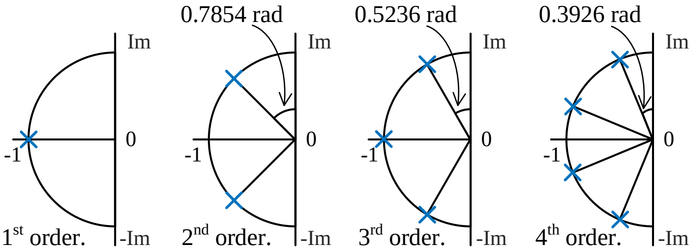

Figure 5. Butterworth root locus.

To obtain the new position of the poles of the augmented fourth-order system, the factor M for tuning has been introduced; this factor multiplies the $|\omega_n|$, which is the magnitude of the open-loop wideband to obtain ω_c which is the magnitude of the closed-loop wideband. The value of the factor M should be selected considering the physical limitations given before. In this paper, $M = 1.8$ for satisfying the limits previously established; hence, we can calculate the proposed closed-loop eigenvalues in the polar form as:

$$\alpha_{\mathrm{i\_ism\_cl}} = |\omega_n| M \angle \left(\frac{\pi}{2n_{\mathrm{ext}}}(2\mathrm{i} - 1) + \frac{\pi}{2} \right) \text{ for i = 1,2,3,4} \tag{19}$$

where n_{ext} is the order of the closed-loop system, 4 in this case.

Figure 6 pinpoints the eigenvalue displacement from open loop to closed loop, keeping its semicircle shape according to Figure 5.

Tuning gains using the Ackerman formula are:

$$\begin{aligned} \mathbf{k} &= \begin{bmatrix} -166.17 & 283.86 & 7.30 \end{bmatrix} \\ \mathrm{k_i} &= -230.63 \times 10^3 \end{aligned} \tag{20}$$

Then, the holistic control law for the three operation modes has the following form:

$$\begin{aligned} v_{ab\mathrm{j}} &= \mathrm{k}_1 x_1 + \mathrm{k}_2 x_2 + \mathrm{k}_3 x_3 + \mathrm{k_i} \sigma_{\mathrm{j}} \\ \dot{\sigma_{\mathrm{j}}} &= x_j^* - x_j \end{aligned} \tag{21}$$

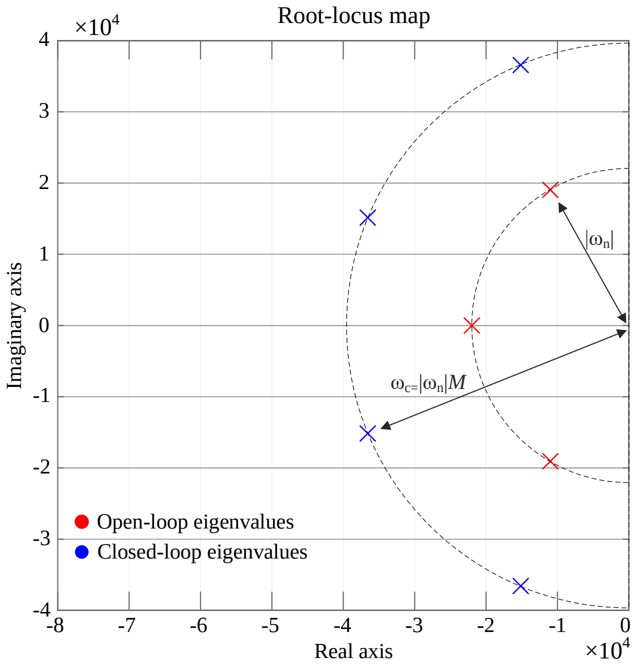

Figure 6. Movement of the root locus in closed loop.

Table 3 summarizes $\hat{\mathbf{A}}$ and the closed-loop eigenvalues for each mode. As can be seen, all the eigenvalues have a negative real part and are constrained by the physical frequency boundaries of the system explained before.

The control law (21) is used by the three legs of the three-phase full-bridge converter by shifting 120° and 240°, respectively.

Table 3. Closed-loop matrices and eigenvalues.

Operation	**Closed-Loop**	**Eigenvalues**
Mode	**Matrix**	**(rad/s)**
Islanded mode	$\hat{\mathbf{A}}_{\mathrm{ism}}$	$\alpha_{1,2\_\mathrm{ism\_cl}} = -36.55 \pm j15.13 \times 10^3$ $\alpha_{3,4\_\mathrm{ism\_cl}} = -15.13 \pm j36.54 \times 10^3$
Grid-connected mode (inverter)	$\hat{\mathbf{A}}_{\mathrm{gci}}$	$\alpha_{1\_\mathrm{gci\_cl}} = -36.02 \times 10^3$ $\alpha_{2,3\_\mathrm{gci\_cl}} = (-33.49 \pm j42.08) \times 10^3$ $\alpha_{4\_\mathrm{gci\_cl}} = -335$
Grid-connected mode (rectifier)	$\hat{\mathbf{A}}_{\mathrm{gcr}}$	$\alpha_{1,2\_\mathrm{gcr\_cl}} = (-26.04 \pm j40.69) \times 10^3$ $\alpha_{3,4\_\mathrm{gcr\_cl}} = (-3.65 \pm j1.27) \times 10^3$

where:

$$\hat{\mathbf{A}}_{\mathrm{ism}} = \begin{bmatrix} -59.40 & 34.77 & -1.73 & 48263.88 \\ 0 & -43.94 & 0.62 & 0 \\ 1153.60 & -1153.60 & 0 & 0 \\ 0 & 0 & -0.001 & 0 \end{bmatrix} \times 10^3 \quad (22)$$

$$\hat{\mathbf{A}}_{\text{gci}} = \begin{bmatrix} -59.40 & 34.77 & -1.73 & 48,263.88 \\ 0 & -43.94 & 0.62 & 0 \\ 1153.60 & -1153.60 & 0 & 0 \\ 0 & -0.001 & 0 & 0 \end{bmatrix} \times 10^3 \tag{23}$$

$$\hat{\mathbf{A}}_{\text{gcr}} = \begin{bmatrix} -59.40 & 34.77 & -1.73 & 48,263.88 \\ 0 & 0 & 0.62 & 0 \\ 1153.60 & -1153.60 & 0 & 0 \\ 0 & -0.001 & 0 & 0 \end{bmatrix} \times 10^3 \tag{24}$$

5. Energy Consumption When Changes Occur

To emphasize the merits of the approach presented in this paper and comparing it with the previous research [27], the closed-loop matrices $\hat{\mathbf{A}}$ should be obtained. Considering the parameters of the prototype 617 W, 120 V_{L-L}, the matrices are:

$$\hat{\mathbf{A}}_{\text{ism}_{\text{holistic}}} = \begin{bmatrix} -46.14 & 10.19 & -1.07 & 13408 \\ 0 & -43.94 & 0.62 & 0 \\ 1153.60 & -1153.60 & 0 & 0 \\ 0 & 0 & -0.001 & 0 \end{bmatrix} \times 10^3 \tag{25}$$

$$\hat{\mathbf{A}}_{\text{gci}_{\text{holistic}}} = \begin{bmatrix} -46.14 & 10.19 & -1.07 & 13408 \\ 0 & -43.94 & 0.62 & 0 \\ 1153.60 & -1153.60 & 0 & 0 \\ 0 & -0.001 & 0 & 0 \end{bmatrix} \times 10^3 \tag{26}$$

$$\hat{\mathbf{A}}_{\text{gcr}_{\text{holistic}}} = \begin{bmatrix} -46.14 & 10.19 & -1.07 & 13408 \\ 0 & 0 & 0.62 & 0 \\ 1153.60 & -1153.60 & 0 & 0 \\ 0 & -0.001 & 0 & 0 \end{bmatrix} \times 10^3 \tag{27}$$

with:

$$\begin{aligned} \mathbf{k}_{\text{holistic}} &= \begin{bmatrix} -48.72 & 2.20 & 4.16 \end{bmatrix} \\ \mathrm{k}_{\mathrm{i}_{\text{holistic}}} &= -64.07 \times 10^3 \end{aligned} \tag{28}$$

Table 4 shows the analytical comparison of both tuning procedures to demonstrate the merits of this complete Butterworth closed-loop tuning.

Table 4. Analytical comparison between improved holistic control and holistic control approaches.

Holistic Approach [27]	**Improved Holistic Approach**
$\mathrm{M} = 1.8$ and $\omega_n = 21.97\ \mathrm{krad/s}$	$\mathrm{M} = 1.8$ and $\omega_n = 21.97\ \mathrm{krad/s}$
Closed-loop state-feedback tuning : $\alpha_{\mathrm{i\_ism\_cl}} = \mathrm{M} \times \alpha_{\mathrm{i\_ism}}$ for i = 1,2,3 $\alpha_{\mathrm{4\_ism\_cl}} = \dfrac{1}{\mathrm{M}} \times \omega_n$	Closed-loop state-feedback tuning : $\alpha_{\mathrm{i\_ism\_cl}} = \lvert\omega_n\rvert M\angle\left(\dfrac{\pi}{2n_{\mathrm{ext}}}(2\mathrm{i}-1) + \dfrac{\pi}{2}\right)$ for i = 1,2,3,4
$\alpha_{\mathrm{1\_ism\_cl}} = (-39.55) \times 10^3$ $\alpha_{\mathrm{2,3\_ism\_cl}} = (-19.77 \pm j34.25) \times 10^3$ $\alpha_{\mathrm{4\_ism\_cl}} = (-10.98) \times 10^3$ $\lvert\alpha_{\mathrm{1,2,3\_ism\_cl}}\rvert = -39.55 \times 10^3$ $\lvert\alpha_{\mathrm{4\_ism\_cl}}\rvert = -10.98 \times 10^3$	$\alpha_{\mathrm{1,2\_ism\_cl}} = (-36.55 \pm j15.13) \times 10^3$ $\alpha_{\mathrm{3,4\_ism\_cl}} = (-15.13 \pm j36.55) \times 10^3$ $\lvert\alpha_{\mathrm{1,2,3,4\_ism\_cl}}\rvert = -39.55 \times 10^3$
$\mathbf{k}_{\mathrm{holistic}} = \begin{bmatrix} -48.72 & 2.20 & 4.16 \end{bmatrix}$ $\mathrm{k}_{\mathrm{i}_{\mathrm{holistic}}} = -64.07 \times 10^3$	$\mathbf{k} = \begin{bmatrix} -166.17 & 283.86 & 7.30 \end{bmatrix}$ $\mathrm{k_i} = -230.63 \times 10^3$
Root locus of $\alpha_{\mathrm{1,2,3,4\_ism\_cl}}$ 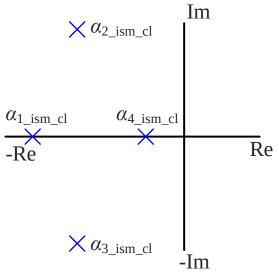 	Root locus of $\alpha_{\mathrm{1,2,3,4\_ism\_cl}}$ 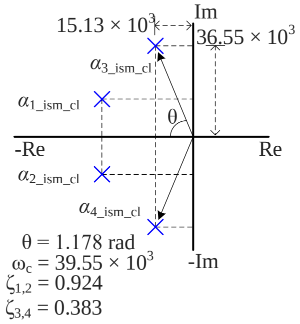
As it can be seen, the dominant pole is overdamped; therefore, its step response is slow and energy wasting as Figure 7 shows.	As it can be seen, the dominant poles are underdamped; therefore, its step response is faster, and the energy transferred is improved than in [27].

Furthermore, to expose the merits of each gain tuning regarding the furnish with the energy, a test protocol with input steps, mode changes, and load steps is performed according to the timeline of Table 5. To develop the protocol test, Equation (18) was implemented using Matlab Simulink.

The BESS philosophy of functioning implies an effort to improve as the energy transfer of the grid-connected converter as the transient response velocity. Thus, Table 5 reveals the improvement in the energy supplied using the proposed approach in all of the scenarios involved. Although columns 4 and 5 show a clearly better performance of the proposed approach, a suggested term of energy efficiency has been introduced as:

$$\eta = \frac{E_{holistic} - E_{improved\_holistic}}{E_{holistic}} \times 100\% \tag{29}$$

with:

$$E_{improved\_holistic} = \int_{t_{event}}^{t_{improved\_holistic}} \left| P_{ab}^{*} - P_{ab\_improved\_holistic} \right| dt \quad (30)$$

$$E_{holistic} = \int_{t_{event}}^{t_{holistic}} \left| P_{ab}^{*} - P_{ab\_holistic} \right| dt \quad (31)$$

where:

- $E_{improved\_holistic}$ is the energy required by the improved holistic controller presented in this paper.
- $E_{holistic}$ is the energy required for the holistic controller given in [27].
- P_{ab}^{*} is the power at steady state due to the voltage and current reference, respectively.
- $P_{ab\_holistic}$ is the power delivered by the holistic control.
- $P_{ab\_improved\_holistic}$ is the power delivered by the improved holistic control.
- t_{event} is the time at the event occurrence (Column 1, Table 5).
- $t_{improved\_holistic}$ is the settling time where the error is $< 1\%$.

$t_{holistic}$ is the settling time where the error is $< 1\%$.

Table 5. Test protocol for improved holistic and holistic closed-loop system comparison.

Time (s)	Type of Event	Change Value According to the Event	Holistic Energy (J)	Improved Holistic Energy (J)	Energy Efficiency (%)
0.1	Voltage step ISM	$r_{\mathrm{ism}} = 0$ V to $r_{\mathrm{ism}} = 120$ V	22.58 m	19.87 m	12.00
0.2	Load transient ISM	$Z_{AB} = 70\ \Omega$ to $Z_{AB} = 35\ \Omega$	16.71 m	12.14 m	27.34
0.3	Mode change ISM-GCI	$r_{\mathrm{ism}} = 120$ V to $r_{\mathrm{gci}} = 1.71$ A	1.38	0.42	69.21
0.4	Current step GCI	$r_{\mathrm{gci}} = 1.71$ A to $r_{\mathrm{gci}} = 2.57$ A	4.80	1.48	69.16
0.5	Load transient GCI	$Z_{AB} = 35\ \Omega$ to $Z_{AB} = 70\ \Omega$	29.08	11.13	61.72
0.6	Mode change GCI-GCR	$r_{\mathrm{gci}} = 2.57$ A to $r_{\mathrm{gcr}} = -1.71$ A	24.22	2.40	90.09

According to Table 5, Figure 7 shows a voltage step response from $r_{\mathrm{ism}} = 0$ V to $r_{\mathrm{ism}} = 120$ V, to reach the rating power. The holistic control uses 22.58 mJ, while the improved holistic control uses 19.87 mJ, with a difference of 12.00% less energy during the transient response.

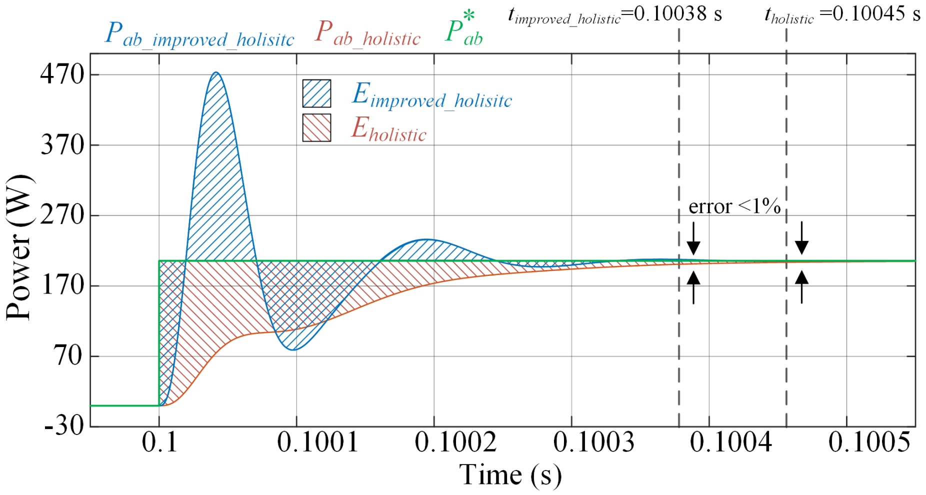

Figure 7. Voltage step response in ISM going from 0 W to 205.7 W.

In Figure 8, the transient occurs at 0.2 s, where there is a load change from $P^*_{ab} = 205.7$ to $P^*_{ab} = 414.4$, which leads the system at twice the supplied power. The holistic control uses 16.71 mJ, while the improved holistic control uses 12.14 mJ, with a difference of 27.34% less energy during the transient response.

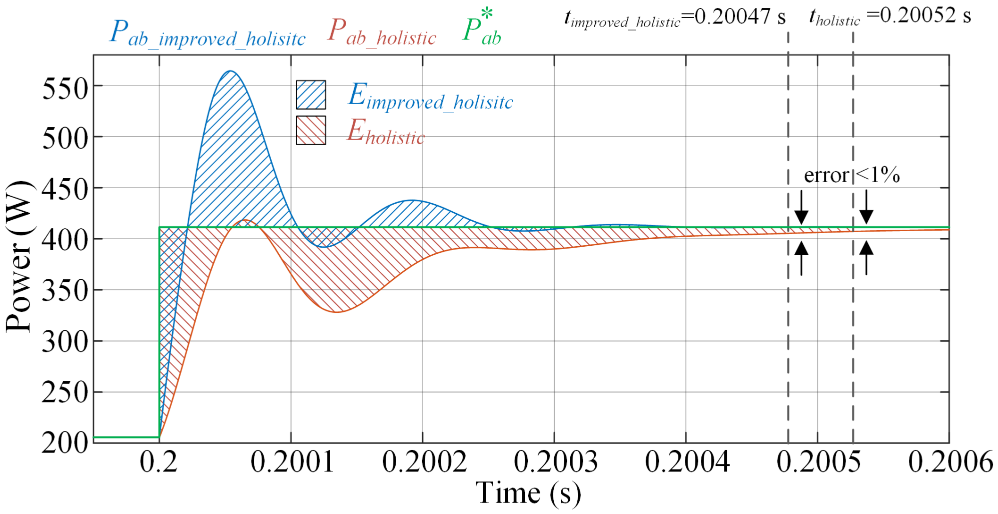

Figure 8. Load transient in ISM going from 205.7 W to 414.4 W.

Figure 9 shows a change from the islanded operation mode to the grid-connected mode as the inverter. In the ISM, the reference is a voltage of $r_{\mathrm{ism}} = 120$ V, but in the GCI, the reference is a current of $r_{\mathrm{gci}} = 1.71$ A. This also implies a power change where the holistic control uses 1.38 J, while the improved holistic control uses 0.42 J, giving a difference of 69.21% less energy during the change mode.

Now, in the GCI mode, a current step occurs at 0.4 s, presented in Figure 10, while a load transient occurs at 0.5 s, presented in Figure 11. In the current step, the holistic control uses 4.80 J, while the improved holistic control uses 1.48 J, giving an efficiency of 69.16%. In the load transient, the holistic control uses 29.08 J, while the improved holistic control uses 11.13 J, giving an efficiency of 61.72%.

To finalize the timeline, at 0.6 s, a mode change occurs, as can be seen in Figure 12, changing from GCI to GCR. In the GCI, the current reference is positive $r_{\mathrm{gci}} = 2.57$ A, but the in GCR, the current is negative $r_{\mathrm{gcr}} = -1.71$ A, denoting the direction change in the current. In this event, the holistic control uses 24.22 J, while the improved holistic control uses 2.40 J, giving an energy efficiency of 90.09%.

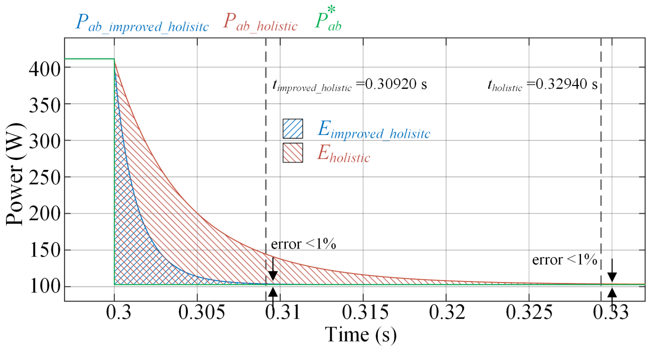

Figure 9. Change from ISM to GCI going from 411.4 W to 102.8 W, respectively.

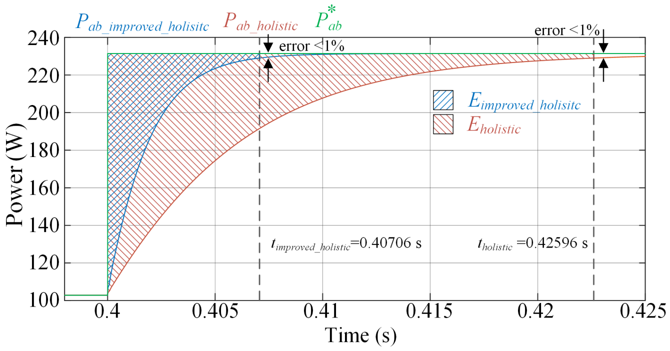

Figure 10. Current step in GCI going from 102.8 W to 231.4 W.

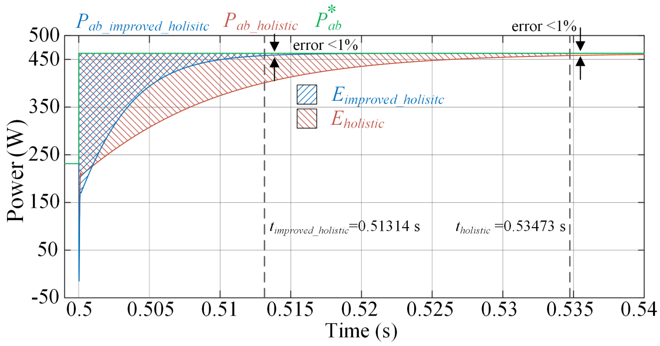

Figure 11. Load transient in GCI going from 231.4 W to 462.8 W.

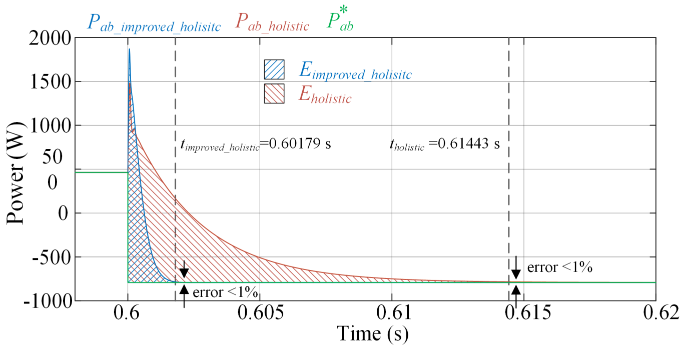

Figure 12. Change from GCI to GCR from 462.8 W to −791.8 W.

The most striking observation to emerge from the data comparison from all the events presented was how a subtle difference in the control tuning that takes into account a concatenated integrator and state-feedback gains into the Butterworth polynomial can represent a remarkable improvement in the required energy and transient velocity for mode changes, load transients, and input steps.

6. Simulation and Experimental Results of the Improved Holistic Control

Following the analytical validation of the holistic control feasibility, a test protocol for the grid-connected converter of a BESS is established in order to present all the transition operation modes and demonstrate the seamless transition behavior. Considering the standard IEEE 1547-2018, the authors delimit the meaning of the seamless transition among the modes as long as the transients do not exceed the continuous operation capability threshold.

6.1. Simulation Results

Figure 13 shows the whole BESS scheme that was used in the PSCAD/EMTDC simulations. The cyan dashed line on the left envelops a schematic circuit that functions as a DC/DC converter and battery simplification. The main objective is to evaluate the seamless transition in the AC side. Complementary to the inverter operation, it is important to say that for the rectifier operation, a voltage regulation of V_{DC} is required. For producing power transients in that mode, BRK$_1$ is opened, and BRK$_2$ and BRK$_3$ make load changes to test the DC voltage regulation capability. Table 6 gives the grid-connected converter electrical parameters to be fulfilled and the LCL filter parameters.

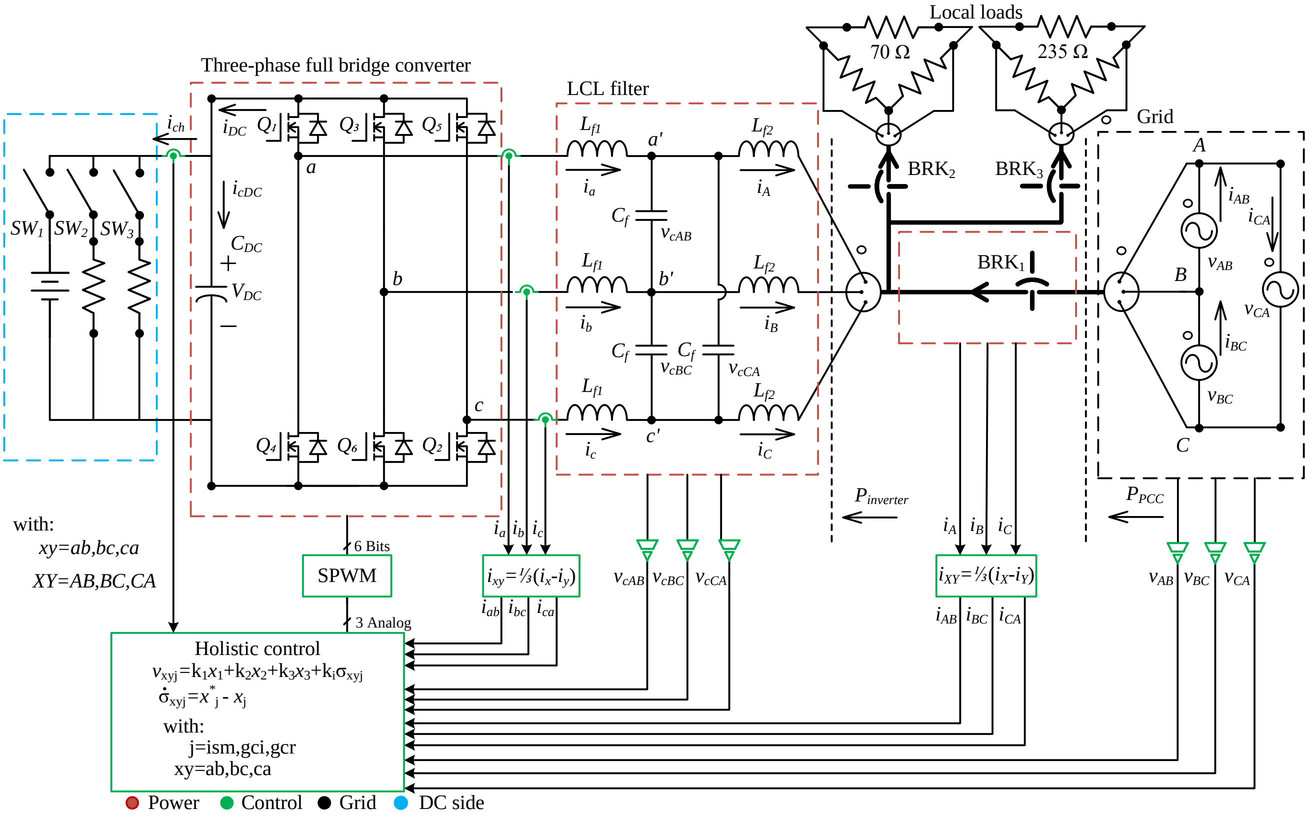

Figure 13. Whole BESS scheme used for simulations.

Table 6. LCL filter and grid-connected converter electrical parameters.

Parameter	**Value**
Grid voltage (AC: L-L, RMS)	120 V
Rated power	617 W
Power factor	Near to unity
V_{DC}	300 V (±3%)
THD of current (i_{AB}, i_{BC}, i_{CA})	<5%
THD of voltage (v_{AB}, v_{BC}, v_{CA})	<5%
Switching frequency	12,060 Hz
Delta-LCL filter: $\left(L_{f1}, L_{f2}, C_f\right)$	(1.59 mH, 530.95 µH 2.60 µF)
Tuning gains	$\mathbf{k} = \begin{bmatrix} -166.17 & 283.86 & 7.30 \end{bmatrix}$ $\mathrm{k_i} = -230.63 \times 10^3$

To follow the test protocol, consider Table 7 where a timeline is broken down, including all the operation mode changes. The mode changes are controlled by the breakers BRK$_1$, BRK$_2$, and BRK$_3$, because islanded mode detection techniques are not considered in this paper.

Table 7. Test protocol according to timeline.

Time (s)	**Mode**	P_{base} **= 617 W**	**BRK$_1$**	**BRK$_2$**	**BRK$_3$**
0–0.1	Grid-connected mode inverter	−1.47 p.u.	Closed	Closed	Open
0.1–0.3	Grid-connected mode inverter	−1.11 p.u.	Closed	Closed	Open
0.3–0.5	Islanded mode	−1.11 p.u.	Open	Closed	Open
0.5–0.7	Islanded mode	−1.44 p.u.	Open	Closed	Closed
0.7–1.0	Islanded mode	−1.11 p.u.	Open	Closed	Open
1.0–1.2	Grid-connected mode inverter	−1.11 p.u.	Closed	Closed	Open
1.2–1.6	Grid-connected mode rectifier	1.07 p.u.	Closed	Closed	Open
1.6–1.7	Grid-connected mode rectifier	1.31 p.u.	Closed	Open	Open

Following the description of the test protocol for the simulation on the PSCAD, the simulation results are presented as follows: Figure 14 shows the system frequency ride-through on the PCC, and Figure 15 shows the system voltage ride-through at the PCC, both according to IEEE 1547-2018 [22].

Figure 14 shows the required limits for the abnormal frequency ride-through for distributed energy resources and the superimposed frequency simulation result based on Table 7. It can be seen that the frequency remains in the "continuous operation capability" zone during all the load transients and mode transitions.

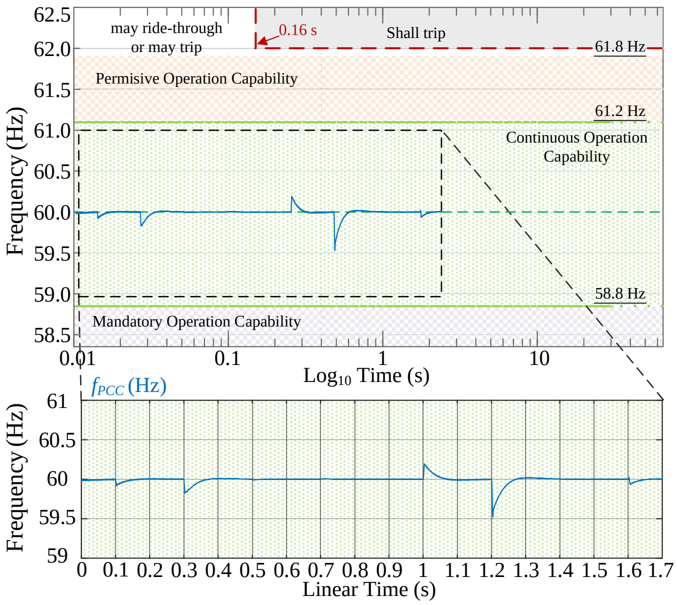

Figure 14. System response on frequency measured at the PCC.

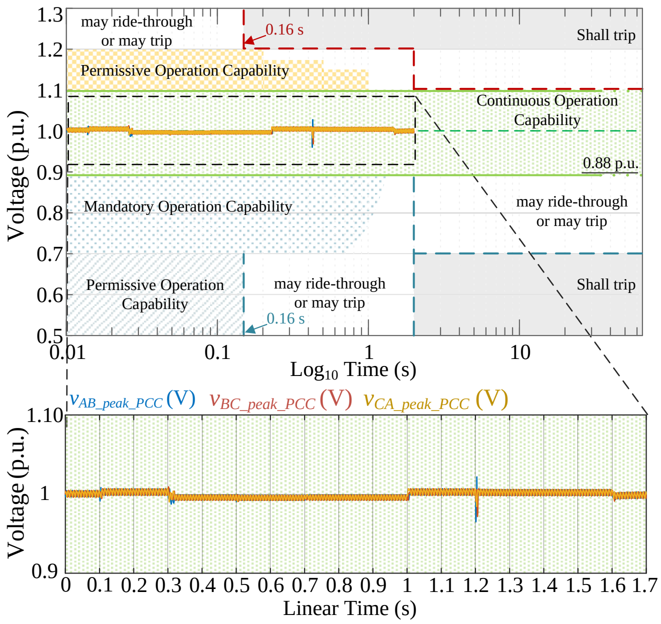

Figure 15. System response in the voltage amplitude measured at the PCC.

According to IEEE 1547-2018, in Figure 15, the required limits for the abnormal voltage ride-through for distributed energy resources are plotted, considering the most restrictive category. In this figure, the simulation result is superimposed to show that the voltage remains in the "continuous operation capability" zone during all the load transients and mode transitions.

Figures 14 and 15 clearly reveal that the improved holistic control confirms the seamless transition for both the load transients and mode transitions.

6.2. Experimental Results

The following step is the validation of the proposal through a laboratory implementation for conceptual testing shown in Figure 16, considering Table 6.

For the prototype experiment, the description is as follows:

- Three power inverters KIT8020CRD8FF1217P-1, SiC mosfet assembly.
- The inductors were built using air core.
- A 400 V, polypropylene capacitor.
- The controller is executed in the dSPACE platform CP1103.

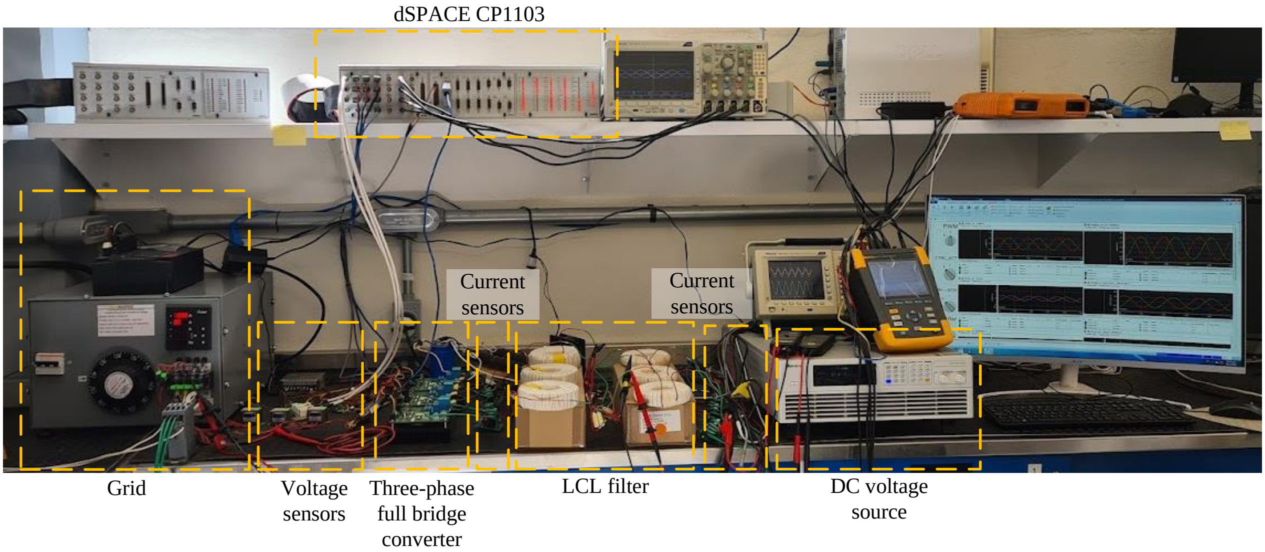

Figure 16. Laboratory implementation.

To evaluate experimentally the seamless transition, the modes highlighted in the gray color in Table 7 are conducted; the transition from the grid-connected mode as an inverter to the islanded mode operation occurred at 0.3 s, the transition from the islanded mode operation to the grid-connected mode as the inverter occurred at 1.0 s, and the transition from the grid-connected mode as an inverter to the grid-connected mode as the rectifier occurred at 1.3 s.

Figure 17 presents the measured waveforms of some selected variables during the transition from the grid-connected mode as an inverter to the islanded mode. Channel 4 in the green line pinpoints the current operation mode of the BESS, channel 1 in navy blue pinpoints the frequency of the voltage at the PCC, channel 2 in cyan pinpoints the (v_{ABrms}), and channel 3 in magenta pinpoints the v_{AB}.

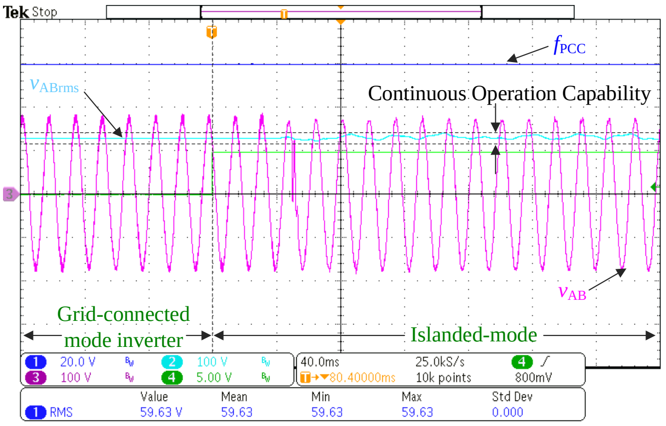

Figure 17. The transition from grid-connected mode to islanded operation mode on the prototype.

Figure 18 presents the operation mode change from the islanded operation mode to the grid-connected mode as an inverter where the channels are ordered in the same way as in Figure 17.

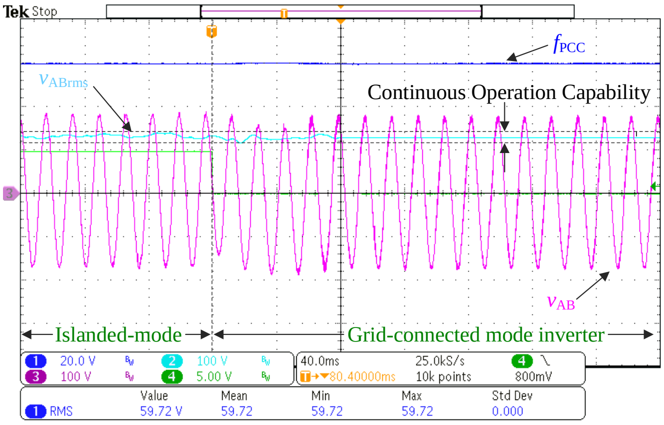

Figure 18. The transition from islanded operation mode to grid-connected mode on the prototype.

Figure 19 shows the transition from the mode connected to the network as an inverter to the mode connected to the network as a rectifier. Channel 4 in the green line pinpoints the current operation mode of the BESS, channel 1 in navy blue pinpoints the frequency of the voltage at the PCC, channel 2 in cyan pinpoints the v_{ABrms}, and channel 3 in magenta pinpoints the i_{AB}. Here, the current i_{AB} is presented to show the 180° phase shift originated by the change in the current direction due to the mode transition.

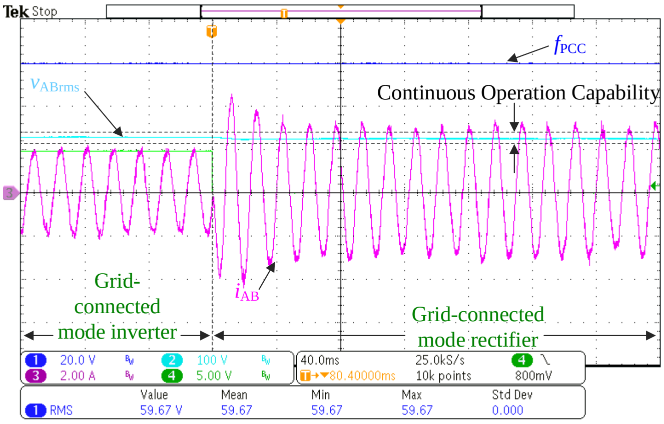

Figure 19. The transition of the current from grid-connected mode as inverter to grid-connected mode as rectifier.

In the three transitions shown in Figures 17–19, it can be seen that the frequency barely has a visible transient, and the voltage amplitude remains within the thresholds of the "continuous operation capability" given by the IEEE-1547-2018 standard. Based on the results presented in this section, the authors demonstrate that the connection between the LCL filter design and control gains tuning as an integrated design process guarantees the seamless transition behavior of the DC/AC power converter at the AC side.

7. Discussion

BESS systems transfer, delay, channel, and improve the electrical energy through power electronics converters that should operate in multiple operation modes. In this paper, the knowledge of the polynomial filter design published in the 1960s in [33] was taken by the authors, and its concept has been extended for the tuning of a closed-loop control under the same polynomial premises, which allows the formulation of an integrated design methodology, obtaining the following contributions:

- Energy efficiency improvement during mode transitions and load transients.
- A test protocol that involves all the mode transitions and load transients on the fly for the experimental validation of the control scheme.
- A seamless transition capability is validated according to IEEE 1547-2018, which guarantees operation in the continuous region limited by the standard.
- One relevant result is the fact that the same polynomial tuning and filter design operates correctly when the converter is used as a rectifier without tuning changes.

Summarizing the concatenated design of the LCL filter BESS with the closed-loop Butterworth polynomial control, Figure 20 shows a flowchart with the step-by-step methodology to obtain improved holistic control.

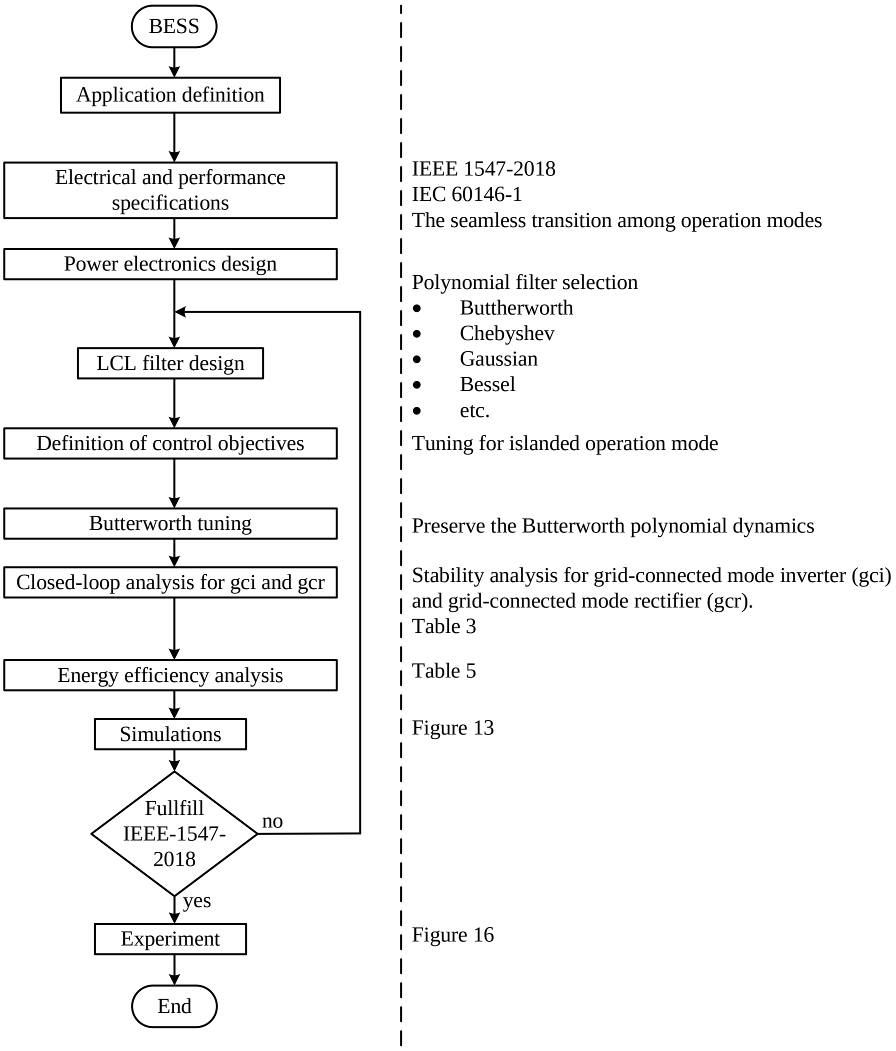

Figure 20. Improved holistic control methodology.

8. Conclusions

The BESS has increased in significance in recent years as it is incorporated into today's distributed electrical systems. Its relevance lies in its flexibility in changing the operating mode and responding to load transients by following a reference set point ordered by the hierarchical control triangle. This paper presents the design method for the LCL filter in more detail under a Butterworth linear polynomial approach, and the closed-loop control tuning now considers the closed-loop system due to the integral action; thus, the Butterworth performance is preserved in the whole system when the tuning gains are designed, and these designs were carried out considering the islanded operation mode. The islanded operation mode was the point of reference because the transfer function fulfills the condition of the dimensional similitude between the input and output, which means the input voltage and output voltage. Unlike the previous research, this method proposes a tuning factor for the closed-loop system, considering the wideband and the switching frequency, which is evidence of the connection between the LCL filter design and control gains tuning as an integrated design process. When the tuning gains are evaluated in each closed-loop matrix, the eigenvalues locus reveals that the system is stable for each operation mode. These results mean that the same tuning gains work for all the operation modes, avoiding gains re-tuning. Unlike the previous paper reported by the authors, this research modifies the root locus of the closed-loop system to establish a complete Butterworth polynomial. This thin difference is motivated by the opportunities for enhancing the energy treatment. The results offer a clear difference when the energy requirements are plotted, representing a better performance generating considerable energy savings whose range moves from 12% to 90%; furthermore, the settling time is highly improved. This finding is relevant when a bulk energy amount needs to be transferred to accomplish power peak shaving, frequency supporting, and islanded operation mode, among others, which inspired the basis for this research. To evaluate the seamless transition, tests were carried out, taking into account the IEEE-1547-2018 standard; the simulations and experiments demonstrated the seamless transition capability when the BESS changes operation modes and load transients.

As future research, formulating other tests which include more scenarios, such as nonlinear loads, virtual inertia, and sub-synchronous resonance compensation, among others, can be developed.

Author Contributions: Conceptualization, C.N.; Investigation, A.A.; Methodology, C.N. and N.V.; Project administration, N.V.; Resources, A.A.V.-F.; Supervision, C.N.; Validation, A.A.; Visualization, A.A.V.-F.; Writing—original draft, A.A.; Writing—review & editing, N.V. and A.A.V.-F. All authors have read and agreed to the published version of the manuscript.

Funding: This research was funded by Consejo Nacional de Ciencia y Tecnología A1-S-29705.

Conflicts of Interest: The authors declare no conflict of interest. The funders had no role in the design of the study; in the collection, analyses, or interpretation of data; in the writing of the manuscript; or in the decision to publish the results.

References

1. IRENA. *Electricity Storage Valuation Framework: Assessing System Value and Ensuring Project Viability*; 2020. Available online: www.irena.org (accessed on 20 August 2022).
2. Venkatesan, K.; Govindarajan, U.; Kasinathan, P.; Padmanaban, S.; Holm-Nielsen, J.B.; Leonowicz, Z. Economic analysis of HRES systems with energy storage during grid interruptions and curtailment in Tamil Nadu, India: A hybrid RBFNoeHo technique. *Energies* **2019**, *12*, 3047. [CrossRef]
3. Lasseter, R. MicroGrids: A Conceptual Solution. In Proceedings of the 2002 IEEE Power Engineering Society Winter Meeting. Conference Proceedings (Cat. No.02CH37309), New York, NY, USA, 27–31 January 2002; Volume 1, pp. 305–308. [CrossRef]
4. Rocabert, J.; Luna, A.; Blaabjerg, F.; Rodríguez, P. Control of Power Electronic Converters in AC Microgrids. *Power Syst.* **2012**, *27*, 329–355. [CrossRef]
5. Karimi-Ghartemani, M.; Khajehoddin, S.A.; Piya, P.; Ebrahimi, M. Universal Controller for Three-Phase Inverters in a Microgrid. *IEEE J. Emerg. Sel. Top. Power Electron.* **2016**, *4*, 1342–1353. [CrossRef]
6. Palizban, O.; Kauhaniemi, K.; Guerrero, J.M. Microgrids in active network management—Part I : Hierarchical control , energy storage , virtual power plants , and market participation. *Renew. Sustain. Energy Rev.* **2014**, *36*, 428–439. [CrossRef]
7. Salehi, N.; Martinez-Garcia, H.; Velasco-Quesada, G.; Guerrero, J.M. A Comprehensive Review of Control Strategies and Optimization Methods for Individual and Community Microgrids. *IEEE Access* **2022**. [CrossRef]
8. D'Silva, S.; Shadmand, M.; Bayhan, S.; Abu-Rub, H. Towards grid of microgrids: Seamless transition between grid-connected and islanded modes of operation. *IEEE Open J. Ind. Electron. Soc.* **2020**, *1*, 66–81. [CrossRef]
9. Bastidas-Rodríguez, J.D.; Ramos-Paja, C. Types of inverters and topologies for microgrid applications. *Rev. Uis Ing.* **2017**, *16*, 7–14. [CrossRef]

10. Somakumar, R.; Kasinathan, P.; Monicka, G.; Rajagopalan, A.; Ramachandaramurthy, V.K.; Subramaniam, U. Optimization of emission cost and economic analysis for microgrid by considering a metaheuristic algorithm-assisted dispatch model. *Int. J. Numer. Model. Electron. Netw. Devices Fields* **2022**, *35*, e2993. [CrossRef]
11. dos Santos Neto, P.J.; Barros, T.A.; Silveira, J.P.; Filho, E.R.; Vasquez, J.C.; Guerrero, J.M. Power management techniques for grid-connected DC microgrids: A comparative evaluation. *Appl. Energy* **2020**, *269*, 115057. [CrossRef]
12. Zhang, Y.; Yang, P.; Xu, Z.; Chen, J. Smooth mode transition strategies of PV-BESS microgrids. In Proceedings of the 2017 2nd International Conference on Power and Renewable Energy, ICPRE 2017, Chengdu, China, 20–23 September 2017; pp. 709–716. [CrossRef]
13. Cucuzzella, M.; Incremona, G.P.; Ferrara, A. Design of Robust Higher Order Sliding Mode Control for Microgrids. *IEEE J. Emerg. Sel. Top. Circuits Syst.* **2015**, *5*, 393–401. [CrossRef]
14. Zhang, L.; Dong, Y.; Chen, Z.; Xie, X.; Sun, H.; Liu, Z. An integrated control strategy of battery energy storage system in microgrid. *IET Conf. Publ.* **2013**, *2013*, 2–40. [CrossRef]
15. Fusero, M.; Tuckey, A.; Rosini, A.; Serra, P.; Procopio, R.; Bonfiglio, A. A comprehensive inverter-bess primary control for AC microgrids. *Energies* **2019**, *12*, 3810. [CrossRef]
16. Zafar, S.; Sadiq, H.; Javaid, B.; Khalid, H.A. On PQ control of BESS in grid-connected mode and frequency control in Islanded-mode for micro-grid application. In Proceedings of the 2018 International Conference on Computing, Electronic and Electrical Engineering, ICE Cube 2018, Quetta, Pakistan, 8–9 October 2018; pp. 1–6. [CrossRef]
17. Shan, S.; Umanand, L. A Unified Controller for Utility-Interactive Uninterruptible Power Converters for Grid Connected and Autonomous Operations. *IEEE Trans. Power Electron.* **2019**, *34*, 3871–3887. [CrossRef]
18. Bayhan, S.; Abu-Rub, H. A Simple Control Technique for Distributed Generations in Grid-Connected and Islanded Modes. *IEEE Int. Symp. Ind. Electron.* **2018**, *2018*, 1237–1242. [CrossRef]
19. Onar, B.; evki Demirbas, S. A Survey on the Provision of Smooth Transition between Operation Modes in PV-BESS Microgrid. In Proceedings of the 2022 10th International Conference on Smart Grid (icSmartGrid), Singapore, 25–28 October 2022; Institute of Electrical and Electronics Engineers (IEEE): Piscataway, NJ, USA, 2022; pp. 203–207. [CrossRef]
20. Kannan, S.; Gnanasekar, R.K.; Vasudevan, K. Novel Unified Control Strategies for Seamless Transfer of Operation of Three-Phase Pv-Inverter From Grid-Tied To Islanded Mode. In Proceedings of the CIRED, Ljubljana, Slovenia, 7–8 June 2018; pp. 7–8.
21. Jaga, O.P.; Choudhuri, S.G. Seamless Transition between Grid-Connected and Islanded Operation Modes for Hybrid PV-BESS Combination Used in Single-Phase, Critical Load Applications. In Proceedings of the 2021 International Conference on Sustainable Energy and Future Electric Transportation (SEFET), Hyderabad, India, 21–23 January 2021. [CrossRef]
22. *IEEE 1547-2018*; IEEE Standard for Interconnection and Interoperability of Distributed Energy Resources with Associated Electric Power Systems Interfaces Sponsored by the IEEE Standard for Interconnection and Interoperability of Distributed Energy Resources with Associate. IEEE: New York, NY, USA, 2018.
23. Sindhuja, I.; Latha, Y.K.; Aparna, V. A unified seamless transfer control scheme for grid-connected and islanding modes of operation of grid- connected PV system. *Indian J. Sci. Technol.* **2016**, *9*, 1–8. [CrossRef]
24. Liu, Z.; Liu, J. Indirect current control based seamless transfer of three-phase inverter in distributed generation. *IEEE Trans. Power Electron.* **2014**, *29*, 3368–3383. [CrossRef]
25. Mao, M.; Dong, Z.; Ding, Y.; Chang, L. A unified controller for A microgrid based on adaptive virtual impedance and conductance. In Proceedings of the 2014 IEEE Energy Conversion Congress and Exposition, ECCE 2014, Pittsburgh, PA, USA, 14–18 September 2014; pp. 695–701. [CrossRef]
26. Ganjian-Aboukheili, M.; Shahabi, M.; Shafiee, Q.; Guerrero, J.M. Seamless Transition of Microgrids Operation from Grid-Connected to Islanded Mode. *IEEE Trans. Smart Grid* **2020**, *11*, 2106–2114. [CrossRef]
27. Nunez, C.; Visairo-Cruz, N.; Arellanes, A.; Mora, D.; Segundo, J. Holistic Control Approach for the Grid-Connected Converter of a Battery Energy Storage System. *IEEE Access* **2020**, *8*, 216844–216855. [CrossRef]
28. Li, Z. Design and analysis of improved Butterworth low pass filter. In Proceedings of the 2007 8th International Conference on Electronic Measurement and Instruments, ICEMI, Xi'an, China, 16–19 August 2007; pp. 1729–1732. [CrossRef]
29. Laghari, W.M.; Baloch, M.U.; Mengal, M.A.; Shah, S.J. Performance Analysis of Analog Butterworth Low Pass Filter as Compared to Chebyshev Type-I Filter, Chebyshev Type-II Filter and Elliptical Filter. *Circuits Syst.* **2014**, *5*, 209–216. [CrossRef]
30. Sandhu, M.; Kaur, S.; Kaur, J. A Study on Design and Implementation of Butterworth , Chebyshev and Elliptic Filter with MatLab. *Int. J. Emerg. Technol. Eng. Res.* **2016**, *4*, 111–114.
31. Jaga, O.P.; Gupta, R.; Jena, B.; GhatakChoudhuri, S. Bi-directional DC/DC Converters Used in Interfacing ESSs for RESs and EVs: A Review. *IETE Tech. Rev.* **2022**, *10*, 1–37. [CrossRef]
32. Butterworth, S. On the Theory of Filter Amplifiers. *Exp. Wirel. Wirel. Eng.* **1930**, *7*, 536–541.
33. Zverev, A.I. *Handbook of Filter Synthesis*; Westinghouse Electric Corporation: New York, NY, USA, 1967.
34. Holmes, D.G.; Lipo, T.A. *Pulse Width Modulation for Power Converters*; Wiley-Interscience: New York, NY, USA, 2010. [CrossRef]
35. Graham, D.; Lathrop, R.C. The synthesis of "optimum" transient response: Criteria and standard forms. *Trans. Am. Inst. Electr. Eng. Part II Appl. Ind.* **2013**, *72*, 273–288. [CrossRef]